Understanding Electromigration in Cu-CNT Composite Interconnects: A Multiscale Electrothermal Simulation Study

Jaehyun Lee, Salim Berrada, Fikru Adamu-Lema, Nicole Nagy, Vihar P. Georgiev, Toufik Sadi, Jie Liang, Raphael Ramos, Hamilton Carrillo-Nunez, Dipankar Kalita, et al.

Understanding Electromigration in Cu-CNT Composite Interconnects: A Multiscale Electro-Thermal Simulation Study

Jaehyun Lee, Salim Berrada, Fikru Adamu-Lema, Nicole Nagy, Vihar P. Georgiev, Toufik Sadi, Jie Liang, Raphael Ramos, Hamilton Carrillo-Nunez, Dipankar Kalita, Katharina Lilienthal, Marcus Wislicenus, Reeturaj Pandey, Bingan Chen, Kenneth B. K. Teo, Goncalo Goncalves, Hanako Okuno, Benjamin Uhlig, Aida Todri-Sanial, Jean Dijon, and Asen Asenov, *Fellow, IEEE*

***Abstract*—In this paper, we report a hierarchical simulation study on the electromigration problem in Cu-CNT composite interconnects. Our work is based on the investigation of the activation energy and self-heating temperature using a multiscale electro-thermal simulation framework. We first investigate the electrical and thermal properties of Cu-CNT composites including contact resistances using the Density Functional Theory and Reactive Force Field approaches, respectively. The corresponding results are employed in macroscopic electro-thermal simulations taking into account the self-heating phenomenon. Our simulations show that although Cu atoms have similar activation energies in both bulk Cu and Cu-CNT composites, Cu-CNT composite interconnects are more resistant to electromigration thanks to the large Lorenz number of the CNTs. Moreover, we found that a large and homogenous conductivity along the transport direction in interconnects is one of the most important design rules to minimize the electromigration.**

***Index Terms*—Cu-CNT composites, Interconnect, Electromigration, Self-heating, Electro-thermal coupling, DFT, Multi-scale simulation**

I. Introduction

DUAL damascene process technology with proper barrier metals such as TaN has been successfully used to fabricate Cu interconnects for the past 20 years [1]–[3]. However, aggressive scaling of dimensions of microchips results in an increase of the resistance in Cu interconnects due to the grain boundary (GBS) and the surface roughness scatterings (SRS) [4]–[6]. Increased resistance of the interconnect causes increased interconnect delay [7]. Moreover, many types of reliability issues arise during both manufacturing process, such as defects and voids [8], and the operation of the device, such as electromigration (EM) [9]–[12]. It is also well-known that the power consumption increases when scaling down the interconnect [13]. Nowadays, these issues must be considered carefully, since the overall performance and reliability of chips are dominated by interconnects [14], [15].

For more than a decade, carbon-based interconnects have attracted attention as a potential future interconnect technology to overcome some of these problems – GBS, SRS, and electromigration [16]–[22]. Indeed, carbon nanotubes (CNTs) and graphene show high ampacity (maximum current-carrying-capacity) and thermal conductivity thanks to their strong C-C bonding [23]–[25]. Ampacity is one of the key figures used to quantify EM. In particular, to prevent capacitance build-up by the barrier metal, Li *et al.* used single- or bi-layer graphene as the Cu diffusion barrier in Cu interconnects and successfully demonstrated their smaller resistivity and longer EM lifetime [26].

More promising results were shown by Subramaniam *et al.* in 2013 with CNTs [19]. They reported that Cu-CNT composite interconnects without the diffusion barrier can have not only a similar conductivity to Cu interconnects but also a 100 times better ampacity than Cu interconnects. However, an in-depth analysis of the migration reduction of Cu atoms in Cu-CNT composite interconnects is still lacking.

In this paper, we present a multi-scale electro-thermal simulation study to understand the electromigration phenomenon in Cu-CNT composite interconnects. In general, EM in interconnects can be characterized by the Time-To-Fail figure (TTF), whose expression is given by Black's equation [27]:

$$TTF = A^* J^{-r} e^{E_a/(k_B T)} \tag{1}$$

where A^* is an empirical constant, J is the current density, r is a positive dimensionless exponent, k_B is the Boltzmann constant, E_a is the activation energy, and T is the temperature of the interconnect. According to Eq. 1, there are two ways to obtain a larger current density while maintaining the same TTF. The first option is to increase the activation energy. To do this, the diffusion barrier with appropriate properties is adopted in the standard Cu interconnect [3]. The second way is to decrease T, which can be achieved by suppressing the self-heating effects. Unfortunately, decreasing T is difficult

This work was supported by the European Commission EU2020 CONNECT project under grant agreement number 688612.

J.Lee, S. Berrada, F. Adamu-Lema, V. P. Georgiev, H. Carrillo-Nunez, and A. Asenov are with School of Engineering, University of Glasgow, Glasgow, G12 8QQ UK e-mail: Jaehyun.Lee@glasgow.ac.uk

N. Nagy, K. Lilienthal, M. Wislicenus, and B. Uhlig are with Center Nanoelectronic Technologies Department, Fraunhofer, IPMS, 01099 Dresden, Germany

T. Sadi is with the Department of Neuroscience and Biomedical Engineering, Aalto University, P.O. Box 12200, FI-00076 AALTO, Finland

R. Ramos and J. Dijon are with Nanomaterials Department, CEA-LITEN, University of Grenoble Alpes, Grenoble, 38000 France

J. Liang, R. Pandey, and A. Todri-Sanial are with Microelectronics Department, CNRS-LIRMM, Montpellier, 34095 France

D. Kalita and H. Okunol are with Nanomaterials Department, CEA-INAC, University Grenoble Alpes, Grenoble, 38000 France

B. Chen, K. B. K. Teo, and G. Goncalves are with Nanoinstruments Department, AIXTRON Ltd, Cambridge, CB24 4FQ UK

Manuscript received

because the self-heating temperature $\tilde{T}$ is caused by high J or high applied voltage (V) during the chip operation. For this reason, we implemented heat diffusion equation [28] in our simulation framework to capture the self-heating effects. Finally, from all simulation results, we provide design guidelines to optimize the performance of Cu-CNT composite interconnects.

This paper is organized as follow. Section II shows the first principle simulation results of the activation energy and the contact resistance between Cu and CNT. In Section III, we examine the self-heating temperature of Cu and Cu-CNT composite interconnects using the first principle calculation results. In Section IV, we provide the optimal design guidelines for Cu-CNT composite interconnects. Finally, conclusions are drawn in Section V.

II. First principle simulation

We investigated the electrical and thermal properties of Cu-CNT composite interconnects using the Density Functional Theory (DFT) and the Reactive Force Field (ReaxFF) methods, respectively [29]–[33]. Both methods are implemented in the Atomistix Tool Kit (ATK) from QuantumWise [34]. The atomistic structures are optimized until the maximum force of each atom becomes less than 10^{-2} eV/Å for electrical (DFT) and 10^{-4} eV/Å for thermal (ReaxFF) analysis, respectively. For the DFT calculations, we use the Generalized Gradient Approximation (GGA) as the exchange-correlation functional, as proposed by Perdew, Burke, and Ernzerhof [35]. The norm-conserving pseudopotentials generated with the Fritz-Haber Institute pseudopotential code are used with the double-ζ singly-polarized pseudoatomic orbital basis set. The tolerance of the self-consistent field loop calculation is set 10^{-4}.

Fig. 1 illustrates examples of optimized atomistic structures of Cu-CNT(4,4) and Cu-CNT(6,0) composites. The lattice orientation of a Cu part is selected to reduce the lattice mismatch with CNT along the transport direction. We assume that CNT is not strained by Cu in this study. The lattice parameters of bulk Cu, zigzag CNT(6,0), and armchair CNT(4,4) in DFT-GGA calculations are 3.670, 4.280, 2.474 Å, respectively. In addition, we placed Cu atoms to prevent the CNT from being distorted severely.

A. Acitvation energy

The activation energy E_a in Eq. 1, which is the energy required for a thermo-dynamic reaction to occur, is an important parameter to describe the EM phenomenon. In general, the structure with low value of the activation energy is vulnerable to the EM. In 2013, measurements of TTF by Subramaniam *et al.* [19] showed that Cu-CNT composite interconnects exhibit much better EM properties than their Cu counterpart. They attributed this outperformance to the enhancement of Cu's activation energy thanks to the presence of C atoms. Nevertheless, considering the weak van der Waals interaction at the interface between Cu and CNT, it is difficult to see how the presence of the CNT could enhance the activation energy of Cu atoms at its interface. Moreover, in a Cu-CNT composite, there is not only a Cu-CNT interface but also a

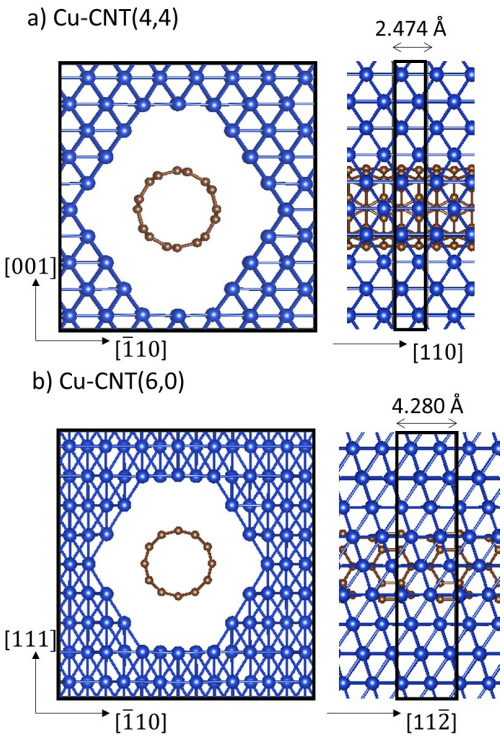

Fig. 1. Atomistic structures of a) Cu-CNT(4,4) and b) Cu-CNT(6,0) composites. The blue and brown spheres are Cu and C atoms, respectively.

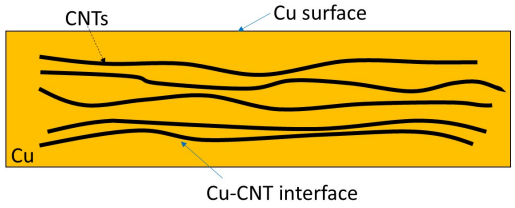

Fig. 2. The schematic diagram of a Cu-CNT composite interconnect [19].

Cu surface, which is the most vulnerable part to the EM in a Cu interconnect as shown in Fig. 2. Consequently, a further theoretical investigation of this phenomenon is needed.

Since the Cu surface in a Cu-CNT composite interconnect is the same as that in a Cu interconnect, we focused on investigating the activation energy at the interface between Cu and CNT. To do this, we constructed a large unit cell by repeating the primitive unit cell 5 times in the transport direction for a Cu-CNT composite interconnect. For bulk Cu, $4 \times 4 \times 4$ face-centered cubic unit cells are created. Moreover, we used the basis set superposition error (BSSE) correction which is usually caused by linear combination of atomic orbital basis (LCAO).

Fig. 3a) shows the three pathways (see read arrows) of the selected Cu atom – marked in yellow – in the Cu-CNT composite structure. This Cu atom is the closest to C atoms; the Cu-C distance (2.178 Å) at the interface in the Cu-CNT composite is shorter than Cu-Cu distance (2.595 Å) in bulk Cu. Fig. 3b) illustrates the potential profile, which is calculated by the total energy difference obtained from

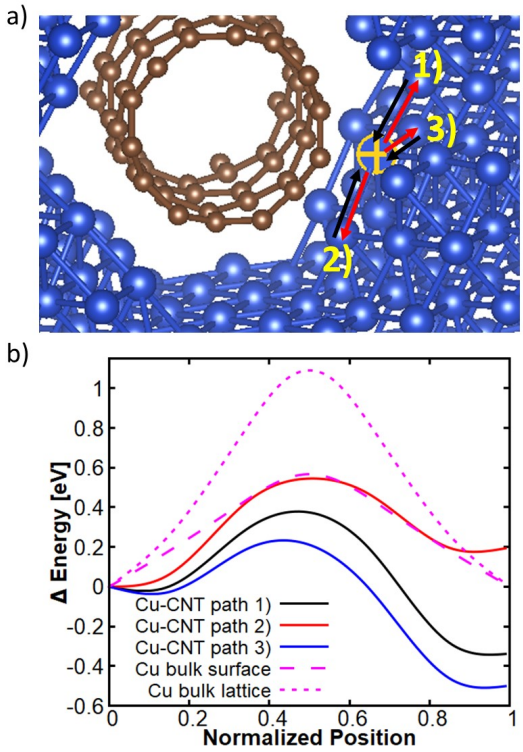

Fig. 3. a) Three pathways where the selected Cu atom (marked in yellow) moves. b) Calculated potential profiles seen by a Cu atom in bulk Cu and a Cu-CNT composite using the DFT-GGA method. For bulk Cu, we calculated the activation energies at the surface and lattice, respectively. The activation energy for each case is the barrier height for the corresponding curves.

DFT-GGA calculations. The potential barriers in this figure indicate the activation energies for Cu atom migration. In the same manner, we calculated the activation energies using the DFT-GGA-D3 approach to correct van der Waals interactions by Grimme D3 [36]. In addition, we estimated the activation energies from the DFT-GGA simulations after removing CNT from a Cu-CNT composite structure. All corresponding results are summarized in Table I.

From all simulation results, it was found that the calculated activation energies at the Cu-CNT interface are not large compared to the activation energies at the surface in bulk Cu (0.567 eV). Moreover, we note again that the surface of a Cu-CNT composite interconnect is still vulnerable to EM like a Cu interconnect. It can, therefore, be concluded that CNT does not contribute significantly to increasing the activation energies of Cu atoms in a Cu-CNT composite interconnect. This is why we need to consider the other parameter in Eq. 1: the temperature.

B. Contact resistance

Fig. 4 shows the schematic diagram of the Cu-CNT composite interconnect used in this study for the macroscopic simulations. As it can be seen from this figure, there are two kinds of contact resistances in the Cu-CNT composite interconnect; end (R_c^{end}) and side contact resistances (R_c^{side}). Due to the low density-of-states (DOS) of CNTs near the Fermi-level, metal-metallic CNT junctions have large contact resistances (R_c), unlike other metal-metal junctions [20], [37]. Therefore, accurate self-heating simulation of Cu-CNT composite interconnects requires a good understanding of the electrical and thermal contact resistances between Cu and CNTs.

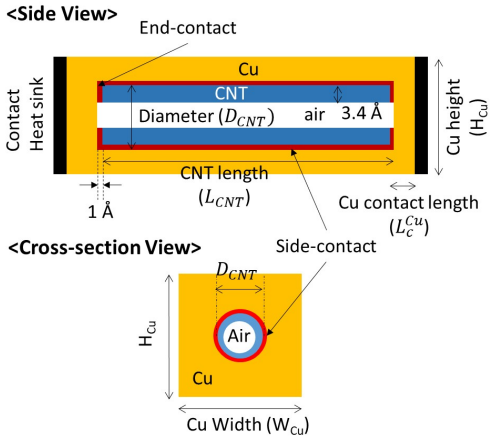

Fig. 4. The schematic diagram of Cu-CNT composite interconnects for a macroscopic electro-thermal simulation. CNT is perfectly surrounded by Cu, and left and right contacts are assumed to be perfect reservoir and heat sink. In the default structure in this study, L_{CNT}, L_c^{Cu}, D_{CNT}, H_{Cu}, and W_{Cu} are 10 μm, 20 nm, 1 nm, 3 nm, and 3 nm, respectively.

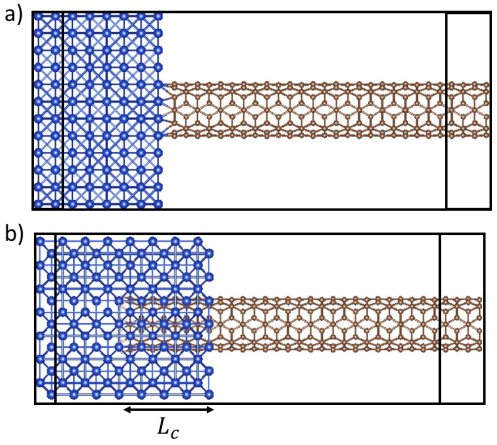

Fig. 5. Atomistic structures to calculate a) the end contact and b) the side contact resistances. Dangling bonds of CNT in the side contact is passivated by hydrogen atoms.

In this study, we used the Non-Equilibrium Green's Function (NEGF) method assuming ballistic transport to calculate the electrical and thermal contact resistances of Cu-CNT junctions. For the sake of computational efficiency, end and side contract resistances are considered separately. The atomistic structures used in this study are shown in Fig. 5. The left end of the CNT in Fig. 5b) is passivated with hydrogen atoms. We used a *k*-point sampling of $1 \times 1 \times 90$.

The end contact resistance R_c^{end} can be extracted from NEGF simulations. Indeed, since the number of conducting channel of bulk Cu near the Fermi-level is much larger than that of single-walled CNT (SWCNT), the total resistance

TABLE I
SUMMARY OF ACTIVATION ENERGIES AT THE CU-CNT INTERFACE IN THE CU-CNT COMPOSITE INTERCONNECT USING THE DFT-GGA AND THE DFT-GGA-D3 APPROACHES. ACTIVATION ENERGIES OF THE CU ATOM WITHOUT CNT ARE ALSO CALCULATED. FOR REFERENCE, WE GOT ACTIVATION ENERGIES OF 1.090 AND 0.567 EV AT THE LATTICE AND THE SURFACE IN BULK CU, RESPECTIVELY FROM DFT-GGA CALCULATIONS. THE NUMBERS IN PARENTHESES ARE THE DIFFERENCE BETWEEN THE ACTIVATION ENERGY AT THE CU-CNT INTERFACE AND THE ACTIVATION ENERGY AT THE SURFACE IN BULK CU.

	Activation energy (eV) at the Cu-CNT interface					
	DFT-GGA calcualtion				DFT-GGA-D3 calculation	
	With CNT		Without CNT		With CNT	
	Red arrow direction	Black arrow direction	Red arrow direction	Black arrow direction	Red arrow direction	Black arrow direction
the 1st pathway	0.374 (-0.193)	0.712 (0.145)	0.205 (-0.362)	0.763 (0.196)	0.320 (-0.247)	0.697 (0.130)
the 2nd pathway	0.545 (-0.022)	0.370 (-0.197)	0.577 (0.010)	0.471 (-0.096)	0.513 (-0.054)	0.315 (-0.252)
the 3rd pathway	0.211 (-0.356)	0.710 (0.143)	0.092 (-0.475)	0.666 (0.099)	0.168 (-0.399)	0.718 (0.151)

TABLE II
ELECTRICAL AND THERMAL CONDUCTIVITIES ARE COMPARED WITH EXPERIMENTAL AND THEORETICAL RESULTS. IN THIS SIMULATION, CU AND CNT(4,4) ARE USED AND ITS ELECTRICAL AND THERMAL CONDUCTIVITIES ARE CALCULATED AT 300K.

	σ S/cm		κ (mW/cm/K)	
	Simulation	Experiment	Simulation	Experiment
End contact	890	33.3 [39], [40]	0.58	0.001-0.045
Side contact	38.2	2.9 [38]	0.29	[41], [42]

R_{total}^{end} of the structure shown in Fig. 5a) reads:

$$R_{total}^{end} = R_{CNT} + R_c^{end}, \tag{2}$$

where R_{CNT} is the ballistic resistance of CNT that we calculated separately. From Eq. 2, we can calculate R_c^{end}. The total resistance of the side contact R_{total}^{side} (see Fig. 5b)) can be expressed as [38]:

$$R_{total}^{side} = R_{CNT} + R_c^{int} + R_c^{side} \tag{3}$$

$$= R_{CNT} + R_c^{int} + \frac{\rho_c^{side}}{\pi D_{CNT} L_c}, \tag{4}$$

where R_c^{int} is the resistance at the interfaces between Cu and Cu-CNT composite and between Cu-CNT composite and CNT, and ρ_c^{side}, D_{CNT}, and L_c are respectively the resistivity of the side contact, the diameter of the CNT, and the overlap length between CNT and Cu as shown in Fig. 5b). R_{total}^{side}'s with different L_c should be calculated to extract ρ_c^{side}.

The thermal contact resistances have been computed from Eqs. 2 and 4 using the ReaxFF method instead of the DFT approach [33]. The calculated electrical (σ) and thermal (κ) conductivities of the end and side contacts for the CNT(4,4) are summarized in Table II with corresponding experimental results from literature [38]–[42]. The calculated results are larger than the experimental results because we considered ideal structures in this simulation study. However, it is noteworthy that such discrepancies do not affect the device simulation results significantly, as discussed later and demonstrated in Fig. 9a). Resistance values obtained for CNTs with other diameters are of the same order of magnitude. Because of the small interaction at the CNT surface, electrical and thermal conductivities at the end contact part are larger than those at the side contact part.

III. MACRSCOPIC SIMULATION

To understand why a Cu-CNT composite interconnect is much more resistant to EM than a Cu interconnect, the self-heating temperature caused by Joule heating should be calculated. The methodology used to perform a self-heating simulation is described in the flowchart shown in Fig. 6. Based on the finite volume discretization scheme, the heat diffusion and current continuity equations are solved self-consistently [28]. The current continuity and heat diffusion equations in steady state are given by:

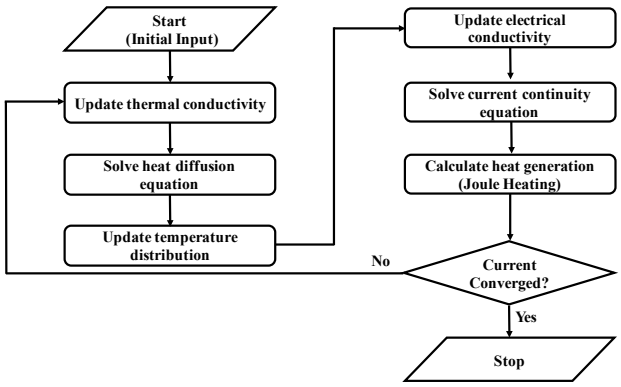

Fig. 6. Flow chart for the electro-thermal steady-state simulation.

$$\nabla \cdot J = \nabla \cdot (\sigma \nabla \varphi) = 0, \tag{5}$$

$$\nabla \cdot (\kappa \nabla T) = -q, \tag{6}$$

where φ is the potential. The heat source q can be written as:

$$q = J \cdot E, \tag{7}$$

where E is electric field.

The electrical conductivity of the CNT (σ_{CNT}) was calculated using the first principle simulations with the mean free path approximation [20], [21]. The conductivity including phonon scattering effects is obtained by introducing the electron mean free path λ:

$$\sigma_{CNT} = \frac{G_{bal} L_{CNT}}{A} \left(1 + \frac{L_{CNT}}{\lambda}\right)^{-1}, \tag{8}$$

where G_{bal} is the ballistic conductance, and L_{CNT} and A are the length and cross-sectional area of the CNT, respectively. In addition, λ of CNT can be given by Matthiessen's Rule [28], [43], [44]:

$$\lambda = \left(\frac{1}{\lambda_{ac}} + \frac{1}{\lambda_{op,ems}^{fld}} + \frac{1}{\lambda_{op,ems}^{abs}} + \frac{1}{\lambda_{op,abs}}\right)^{-1}, \tag{9}$$

where λ_{ac}, $\lambda_{op,ems}^{fld}$, $\lambda_{op,ems}^{abs}$, and $\lambda_{op,abs}$ are the electron mean free paths from acoustic phonon, optical phonon emission after electrons gained energy from the electric field, optical phonon emission after absorption, and optical phonon absorption, respectively. These parameters can be calculated as following [43], [44]:

$$\begin{aligned}
\lambda_{ac} &= 400460 \times \frac{D_{CNT}}{T} \\
\lambda_{op,abs} &= 56.4 \times D_{CNT} \frac{N_{op}(300)+1}{N_{op}(T)} \\
\lambda_{op,ems}^{abs} &= \lambda_{op,abs} + 56.4 \times D_{CNT} \frac{N_{op}(300)+1}{N_{op}(T)+1} \\
\lambda_{op,ems}^{fld} &= \frac{\hbar\omega_{op} - k_B T}{qV/L_{CNT}} + 56.4 \times D_{CNT} \frac{N_{op}(300)+1}{N_{op}(T)+1}
\end{aligned}$$

$N_{OP}(T) = \{1/exp((\hbar\omega_{op})/(k_B T))\} - 1$ is the average optical phonons number defined by the Bose-Einstein distribution, and $\hbar\omega_{op}$ is the optical phonon energy. We set $\hbar\omega_{op}$ to 0.18 eV in this study [44]. The mean free path of CNTs is thus a function of T, L_{CNT} , D_{CNT}, and V.

Using the linear approximation for resistivity, the electrical conductivity of Cu (σ_{Cu}) is given by:

$$\sigma_{Cu}(T) = \frac{\sigma_0}{1 + \alpha(T - T_0)} \tag{10}$$

where T_0 is a fixed reference temperature, 293 K, α = 0.003862 K^{-1} is the temperature coefficient of resistivity and σ_0 is the conductivity at T_0. σ_0 for Cu will be discussed in the next subsection.

We compute the thermal conductivity κ for both Cu and CNT using Wiedemann-Franzs law [45]:

$$\kappa = \sigma \tilde{L} T, \tag{11}$$

where $\tilde{L}$ is the Lorenz number. The values we used for $\tilde{L}$ in this study are 2.23×10^{-8} WΩK^{-2} for Cu [46] and 4.0×10^{-6} WΩK^{-2} for CNT [23]. $\tilde{L}$ of the CNT is about 180 times larger than that of Cu, meaning that the thermal condcutivity κ of the CNT is mostly dominated by phonons (as opposed to Cu where κ is dominated by electrons). In this study, we did not consider heat dissipation through the environment of the interconnects and the calculated $\tilde{T}$ may thus be overestimated. However, this is a global effect affecting all the interconnects considered here and therefore, our study ensures a good comparison between them.

A. Scattering effects in nanoscale Cu interconnect

Fig. 7 shows experimental and theoretical dependence of Cu resistivity ρ_{Cu} on the width of the interconnect W_{Cu} when its height (H_{Cu}) is 90 nm. As expected, the resistivity increases as W_{Cu} decreases due to SRS and GBS effects. To describe these effects, we used the empirical model introduced by Rossnagel *et al.* [6]:

$$\frac{\rho_{Cu}}{\rho_0} = \left\{ 1 + \frac{0.375(1-p)S\lambda}{W_{Cu}} + \frac{1.5\frac{R}{1-R}\lambda}{g} \right\}, \tag{12}$$

where ρ_0 is the bulk Cu resistivity, p is the surface scattering parameter, S is the roughness factor, R is the grain boundary scattering parameter, and g is the average value of grains size. From our experimental data, we successfully extracted the values of the parameters assuming that g is equal to W_{Cu} and the mean free path λ is 40 nm. The parameters are summarized in Table III.

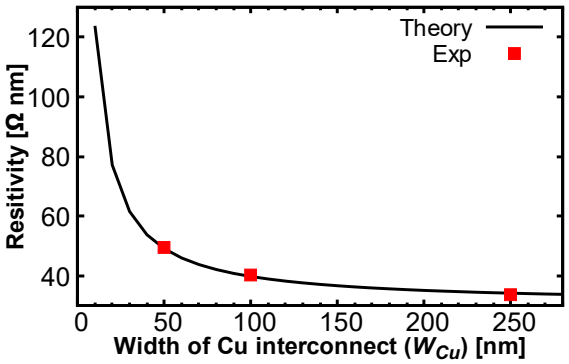

Fig. 7. Experimental and theoretical Cu resistivities versus W_{Cu} when H_{Cu} = 90 nm. The corresponding parameters are summarized in Table III.

TABLE III
PARAMETERS FOR GRAIN BOUNDARY AND SURFACE ROUGHNESS SCATTERING WHEN THE INTERCONNECT HEIGHT H_{Cu} IS 90 NM.

parameters	values
ρ_0	30.42 Ω nm
p	0.816
S	3.762
R	0.253

B. Self-heating effects in Cu and Cu-CNT composite interconnects

We calculated $\Delta\tilde{T}$ as the difference between the maximum self-heating temperature in the device and the temperature of the heat sink (T_{sink} = 300 K). The conductivity and $\Delta\tilde{T}$ resulting from Joule heating with respect to the applied voltage to the Cu and Cu-CNT composite interconnects are depicted in Fig. 8. It shows that self-heating temperature increases more rapidly with the applied bias in the Cu interconnect compared

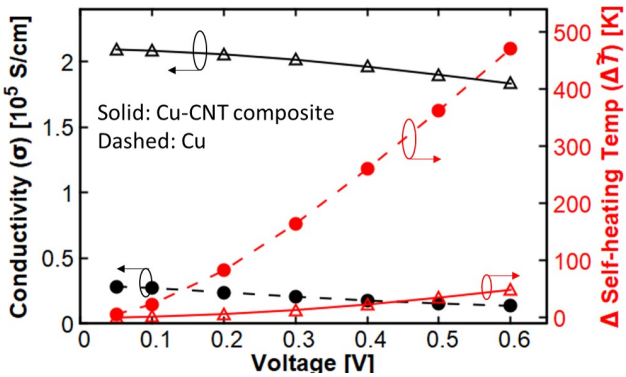

Fig. 8. Calculated conductivity and self-heating temperature difference $\Delta\tilde{T}$ of Cu and Cu-CNT composite interconnects with different applied voltage. L_{CNT}, L_c^{Cu}, D_{CNT}, H_{Cu}, and W_{Cu} are 10 μm, 20 nm, 1 nm, 3 nm, and 3 nm, respectively. The length of Cu interconnect (L_{Cu}) of 10 μm is the same as L_{CNT}.

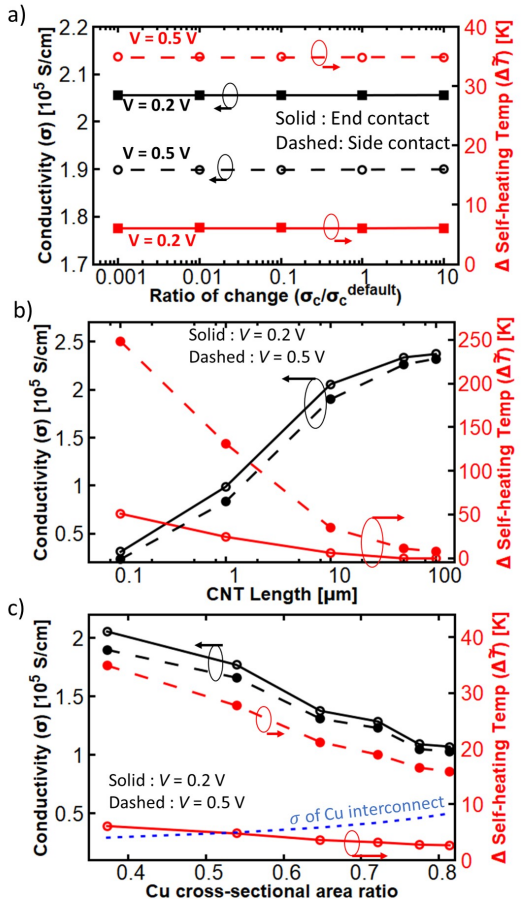

Fig. 9. Variability simulations of Cu-CNT composite interconnects when applying different voltage (0.2 and 0.5 V). We investigated dependence on a) the electrical and thermal conductivities at the end and side contacts, b) the CNT length, and c) the Cu ratio, respectively. All non-displayed structure parameters are default values; L_{CNT} = 10 μm, L_c^{Cu} = 20 nm, D_{CNT} = 1 nm, H_{Cu} = 3 nm, and W_{Cu} = 3 nm.

to the Cu-CNT composite interconnect. We also found that the conductivity of both interconnects is slightly degraded at higher operating temperatures. This behavior results from an increased phonon scattering at higher T. It is important to note that an increase in T and a decrease in σ of interconnects exacerbate the EM. Indeed, the reduction in σ requires a larger electric field to deliver the same current density, which in turn causes the temperature rise in the interconnects; i.e. there is a negative feedback between the self-heating effect and EM. From this point of view, it is clear that Cu-CNT composite interconnects can be stronger against EM than Cu interconnects thanks to its lower self-heating temperature and significantly larger thermal conductivity of CNT.

C. Variablity simulations of Cu-CNT composite interconnect

To gain a deeper insight into self-heating effects in Cu-CNT composite interconnects, we performed variability simulations of σ and $\Delta\tilde{T}$ in terms of the electrical and thermal contact resistances, L_{CNT}, and the Cu ratio. The results are shown in Fig. 9. We found that there is very weak dependence on the electrical and thermal contact resistances. Since the electrical and thermal conductivities at both end and side

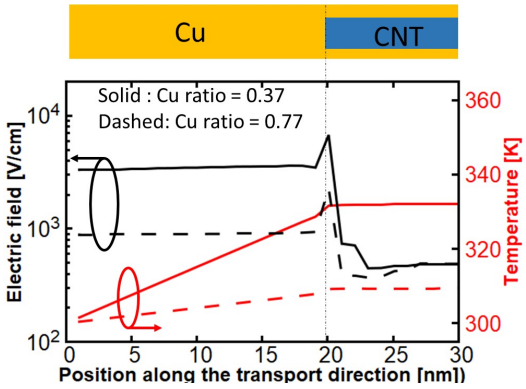

Fig. 10. Calculated electric field and temperature as a function of position along the transport direction near the left contact when Cu ratios are 0.37 and 0.77, respectively at V = 0.5 V. L_{CNT} = 10 μm, L_c^{Cu} = 20 nm, and D_{CNT} = 1 nm.

contacts – calculated by DFT and ReaxFF, respectively – are much smaller than the electrical and thermal conductivities of Cu and CNT, their influence appears to be negligible as shown in Fig. 9a).

The dependence on L_{CNT} is shown in Fig. 9b). As L_{CNT} decreases, σ decreases and $\Delta\tilde{T}$ increases. It is well-known that σ_{CNT} decreases as L_{CNT} decreases due to its large λ [20], [21]. Moreover, as L_{CNT} deceases, the electric field increases. This is the cause of the increase in the self-heating temperature. We also found that Cu-CNT composite interconnects are more beneficial than Cu interconnects when their length becomes shorter. This is because the $\Delta\tilde{T}$ of 0.1 μm length Cu-CNT composite interconnect ($\Delta\tilde{T}$ = 248 K, see Fig. 9b)) is smaller than that of 10 μm length Cu interconnects ($\Delta\tilde{T}$ = 364 K, see Fig. 8)), when V = 0.5 V.

Fig. 9c) shows the self-heating simulation results of σ and $\Delta\tilde{T}$ when D_{CNT} is fixed and H_{Cu} and W_{Cu} are varied from 3 to 5.5 nm. As the Cu ratio increases, both σ and $\Delta\tilde{T}$ decrease. For σ, it is consistent with the general expectations because as Cu becomes increasingly dominant, σ of a Cu-CNT composite interconnect becomes closer to that of a Cu interconnect. However, the calculated $\Delta\tilde{T}$ shows an unexpected behavior. It is highlighted that although a Cu interconnect is suffering more from the self-heating effects as shown in Fig. 8, $\Delta\tilde{T}$ decreases when the Cu ratio becomes large. This behaviour is explained by the build-up of an electric field difference at the interface between the Cu contact and the Cu-CNT composite (see Fig. 4). Fig. 10 depicts the electric field and temperature along the transport direction. Two important conclusions can be drawn from this figure. Firstly, the temperature rise in both interconnects occurs in the Cu contact part. Secondly, when the Cu ratio is higher, the electric field at the Cu contact part is smaller because σ of Cu-CNT composite is similar to that of Cu. Therefore, to decrease the self-heating temperature in interconnects, it is very important to ensure a small variation of the electrical conductivity along the transport direction. This will prevent the build-up of a large electric field at the regions where σ is small.

Only ideal CNTs were considered so far. Since measured conductivities in CNTs are usually lower than the ideal values,

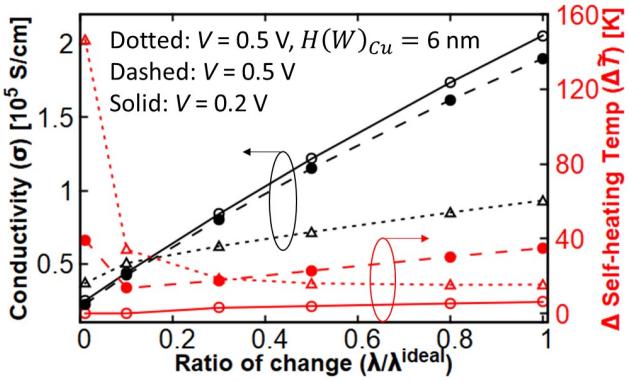

Fig. 11. Calculated conductivity and self-heating temperature difference $\Delta\tilde{T}$ as the mean free path of CNTs is degraded. All non-displayed structure parameters are default values; L_{CNT} = 10 μm, L_c^{Cu} = 20 nm, D_{CNT} = 1 nm, H_{Cu} = 3 nm, and W_{Cu} = 3 nm.

we also investigated the self-heating effect when the mean free path λ of CNTs is degraded. The dependence of σ and $\Delta\tilde{T}$ on degraded λ is shown in Fig. 11, where λ^{ideal} is given by Eq. 9. As the ratio of change of λ decreases, both σ and $\Delta\tilde{T}$ decrease. The reason behind the decrease of $\Delta\tilde{T}$ despite the poor CNT characteristics is related to the smaller difference of conductivity σ between the Cu contact and the degraded Cu-CNT composite. However, $\Delta\tilde{T}$ increases again at a certain point because the CNT conductivity becomes too different (smaller) from the Cu conductivity. We also found that $\Delta\tilde{T}$ with $H_{Cu} = W_{Cu}$ = 6 nm starts to increase at a larger λ/λ^{idea} ratio because of the small contribution from CNTs.

IV. Design Guidelines for Cu-CNT composite interconnects

All simulation results suggest that a Cu-CNT composite interconnect without the barrier metal is highly resistant to EM thanks to the reduced self-heating, and not due to increased activation energy. We propose the Lorenz number $\tilde{L}$ as a new parameter to assess the self-heating and electromigration. The dependence of $\tilde{L}$ on various parameters is shown in Fig. 12. The linear relationship between $\tilde{L}$ and T in Cu-CNT composite interconnects is consistent with experimental results [19]. The correlation of Figs. 12a) and b) with all previous simulation results shows that $\Delta\tilde{T}$ is always higher for the interconnect with the lower $\tilde{L}$. For example, as L_{CNT} decreases, $\Delta\tilde{T}$ increases (see Fig. 9b)). $\tilde{L}$ follows an inverse trend as it decreases when decreasing the CNT length (Fig. 12b)). Furthermore, $\Delta\tilde{T}$ decreases for L_{CNT} = 10 μm when the Cu ratio or $W(H)_{Cu}$ increases (see Fig. 9c). We observe that the Lorenz number also increases in this case (Fig. 12a)).

To see clearly the relationship between σ, $\Delta\tilde{T}$, and $\tilde{L}$, we investigated the self-heating effect with and without the GBS and the SRS effects while artificially varying $\tilde{L}$ in the Cu interconnect as shown in Fig. 13. Although σ is degraded significantly due to scatterings, $\Delta\tilde{T}$ does not depends on σ. We note that $\Delta\tilde{T}$ is inversely proportional to $\tilde{L}$. We thus rewrite

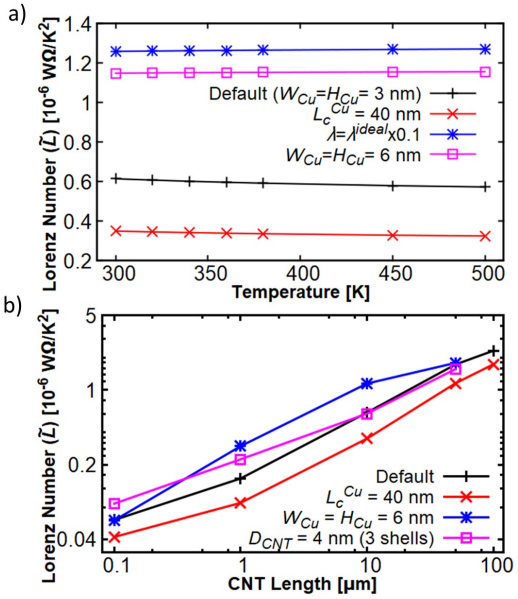

Fig. 12. Simulation study of dependence of the Lorenz number on a) the temperature and b) CNT length. All non-displayed structure parameters are default values; L_{CNT} = 10 μm, L_c^{Cu} = 20 nm, D_{CNT} = 1 nm, H_{Cu} = 3 nm, and W_{Cu} = 3 nm.

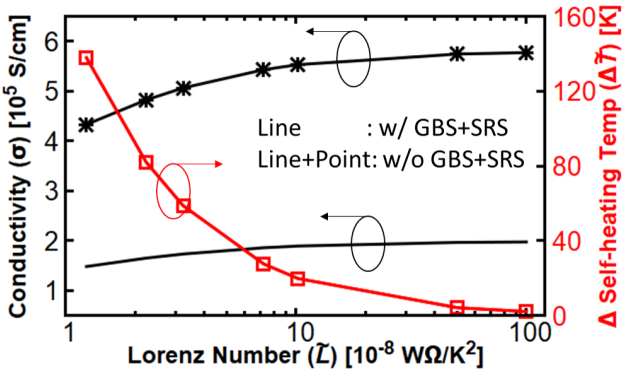

Fig. 13. Calculated conductivity and self-heating temperature difference $\Delta\tilde{T}$ with artificially changed Lorenz number in Cu interconnects with and without grain boundary and surface roughness scattering effects. The interconnect length, width, and height are 10 μm, 50 nm, and 90 nm, respectively. The applied voltage is 0.2 V.

Eq. 1 that will serve as a model to design Cu-CNT composite interconnects:

$$TTF = A^*\{J(\sigma)\}^{-n} e^{\frac{E_a}{k_B(T_{sink}+C/\tilde{L}(\sigma,\kappa))}}, \quad (13)$$

where C is a constant related to the structural information including the homogeneous conductivity.

Taking all the above results together, we can provide three important rules applicable to the design Cu-CNT composite interconnects that show good self-heating properties and are EM resistant. Firstly, interconnects should have a large electrical conductivity. To achieve this, CNTs without defects are desirable in long interconnects. Secondly, interconnects must also possess a high Lorenz number to evacuate the heat more efficiently. Thus, the Cu ratio must be carefully chosen, especially when CNTs are defective. Finally, it is

very important that Cu-CNT composite interconnects have a homogenous conductivity to avoid large electric fields in the regions where σ is discontinuous. Therefore, L_c^{Cu} (as illustrated in Fig. 4) should be minimized.

V. Conclusion

In this work, by comparing experimental data with multi-scale electro-thermal simulations results, we have provided an explanation why Cu-CNT composite interconnects outperform Cu interconnects in terms of electromigration. Our results show that the electromigration is governed by the self-heating related temparature raise, rather than the activation energy of Cu-CNT composites. Also, we have conducted a systematic study which shows that a good Cu-CNT composite interconnect should be designed by co-optimizing the electrical conductivity, the Lorenz number, and the homogenous conductivity. Based on the results obtained from our study, some important modeling and design guidelines have been suggested as follows: large electrical conductivity, large Lorenz number, and homogeneous electrical conductivity to design efficient highly reliable Cu-CNT composite interconnects for aggressively scaled chips. These guidelines could be generalized to other interconnect materials.

References

[1] D. Edelstein, J. Heidenreich, R. Goldblatt, W. Cote, C. Uzoh, N. Lustig, P. Roper, T. McDevittt, W. Motsifft, A. Simon, J. Dukovic, R. Wachnik, H. Rathore, R. Schulz , L. Su, S. Lucet, and J. Slattery, "Full Copper Wiring in a Sub-0.25 pm CMOS ULSI Technology", *in IEDM Tech. Dig., Dec.* 1997, pp. 31.3.1-31.3.4. doi: 10.1109/IEDM.1997.650496

[2] S. Lakshminarayanan, J. Steigerwald, D. T. Price, M. Bourgeois, T. P. Chow, R. J. Gutmann, and S. P. Murarka, "Contact and Via Structures with Copper Interconnects Fabricated Using Dual Damascene Technology", *IEEE Trans. Electron Devices*, vol. 15, no. 8, pp. 307-309, Aug. 1994. doi: 10.1109/55.296225

[3] M.i Hayashi, S. Nakano and T. Wada, "Dependence of copper interconnect electromigration phenomenon on barrier metal materials", *Microelectron. Reliab.*, vol. 43, no. 9-11, pp. 1545-1550, 2003. doi: 10.1016/S0026-2714(03)00273-7

[4] W. Steinhgl, G. Schindler, G. Steinlesberger, M. Traving, and M. Engelhardt, "Comprehensive study of the resistivity of copper wires with lateral dimensions of 100 nm and smaller", *J. Appl. Phys.*, vol. 97, 023706, 2005. doi: 10.1063/1.1834982

[5] A. Pyzyna, H. Tsai, M. Lofaro, L. Gignac, H. Miyazoe, R. Bruce, C. M. Breslin, M. Brink, D. Klaus, M. Guillorn, C. Lavoie, K. P. Rodbell, D.-G. Park, and E. Joseph, "Resistivity of copper interconnects at 28 nm pitch and copper cross-sectional area below 100 nm^2", *in IEEE IITC*, 2017, doi: 10.1109/IITC-AMC.2017.7968982

[6] S. M. Rossnagel and T. S. Kuan, "Alteration of Cu conductivity in the size effect regime", *J. Vacuum Sci. Technol. B, Nanotechnol. Microelectron.*,vol. 22, no. 1, pp. 240247, Jan. 2004. doi: 10.1116/1.1642639

[7] P. Kapur, G. Chandra, J.P. McVittie, and K.C. Saraswat, "Technology and reliability constrained future copper interconnects. II. Performance implications", *IEEE Trans. Electron Devices*, vol. 49, no. 4, pp. 598-604, Apr. 2002. doi: 10.1109/16.992868

[8] M.A. Hussein and Jun He, "Materials' impact on interconnect process technology and reliability", *IEEE Trans. Semicond. Manuf.*, vol. 18, no. 1, pp. 69-85, Feb. 2005. doi: 10.1109/TSM.2004.841832

[9] P. Besser, A. Marathe, L. Zhao, M. Herrick, C. Capasso, and H. Kawasaki, "Optimizing the electromigration performance of copper interconnects", *in IEDM Tech. Dig., Dec.* 2000, pp. 119-122. doi: 10.1109/IEDM.2000.904272

[10] J. R. Lloyd, and J. J. Clement, "Electromigration in copper conductors", *Thin Solid Films*, vol. 262, no. 1-2, pp. 135-141, Jun. 1995. doi: 10.1016/0040-6090(94)05806-7

[11] J. Tao, N.W. Cheung, and C. Hu, "Electromigration characteristics of copper interconnects", *IEEE Electron Device Lett.*, vol. 14, no. 5, pp. 249-251, May 1993. doi: 10.1109/55.215183

[12] H. Chen, C. Huang, C. Wang, W. Wu, C. Liao, L. Chen, and K. Tu, "Optimization of the nanotwin-induced zigzag surface of copper by electromigration", *Nanoscale*, vol. 8, pp. 2584, Jan. 2016. doi: 10.1039/c5nr05418d

[13] Xiao-Chun Li, Jun-Fa Mao, Hui-Fen Huang, and Ye Liu, "Global Interconnect Width and Spacing Optimization for Latency, Bandwidth and Power Dissipation", *IEEE Trans. Electron Devices*, vol. 52, no. 10, pp. 2272-2279, Sep. 2005. doi: 10.1109/TED.2005.856795

[14] IEEE International Roadmap for Devices and Systems report. Available: https://irds.ieee.org/reports [Accessed Dec. 04, 2017].

[15] R.H. Havemann and J.A. Hutchby, "High-performance interconnects: an integration overview", *Proc. IEEE*, vol. 89, no. 5, pp. 586-601, May 2001. doi: 10.1109/5.929646

[16] K. Z. Milowska, M. Ghorbani-Asl, M. Burda, L. Wolanicka, N. ati, P. D. Bristowe, and K. K. K. Koziol, "Breaking the electrical barrier between copper and carbon nanotubes", *Nanoscale*, vol. 9, pp. 8458, Jun. 2017. doi: 10.1039/c7nr02142a

[17] O. Hjortstam, P. Isberg, S. Soderholm, and H. Dai, "Can we achieve ultra-low resistivity in carbon nanotube-based metal composites?", *Appl. Phys. A*, vol. 78, pp. 11751179, Jan. 2004. doi: 10.1007/s00339-003-2424-x

[18] G. Xu, J. Zhao, S. Li, X. Zhang, Z. Yong, and Q. Li, "Continuous electrodeposition for lightweight, highly conducting and strong carbon nanotube-copper composite fibers", *Nanoscale*, vol. 3, pp. 4215, Aug. 2011. doi: 10.1039/c1nr10571j

[19] C. Subramaniam, T. Yamada, K. Kobashi, A. Sekiguchi, D. N. Futaba, M. Yumura, and K. Hata, "One hundred fold increase in current carrying capacity in a carbon nanotubecopper composite", *Nat. Comm.*, vol. 4, pp. 2202, Jul. 2013. doi: 10.1038/ncomms3202

[20] J. Lee, J. Liang, S. M. Amoroso, T. Sadi, L. Wang, P. Asenov, A. Pender, D. T. Reid, V. P. Georgiev, C. Millar, A. Todri-Sanial, and A. Asenov, "Atoms-to-Circuits Simulation Investigation of CNT Interconnects for Next Generation CMOS Technology", *in Proc. SISPAD* 2017, pp. 153-156. doi: 10.23919/SISPAD.2017.8085287

[21] A. Naeemi and J. D. Meindl, "Compact Physical Models for Multiwall Carbon-Nanotube Interconnects", *IEEE Electron Device Lett.*, vol. 27, no. 5, pp. 338-340, May 2006. doi: 10.1109/LED.2006.873765

[22] A. Todri-Sanial, R. Ramos, H. Okuno, J. Dijon, A. Dhavamani, M. Wislicenus, K. Lilienthal, B. Uhlig, T. Sadi, V. P. Georigev, A. Asenov, S. M. Amoroso, A. R. Brown, A. Pender, C. Millar, F. Motzfeld, B. Gotsmann, J. Liang, G. Gonalves, N. Rupesinghe, and K. Teo, "A Survey of Carbon Nanotube Interconnects for Energy Efficient Integrated Circuits", *IEEE Circuits Syst. Mag.*, vol. 17, no. 2, pp. 47-62, May 2017. doi: 10.1109/MCAS.2017.2689538

[23] J. Hone, M. Whitney, C. Piskoti, and A. Zettl, "Thermal conductivity of single-walled carbon nanotubes", *Phys. Rev. B*, vol. 59, no. 4, pp. R2514, Jan. 1999. doi: 10.1103/PhysRevB.59.R2514

[24] S. Berber, Y. Kwon, and D. Tomnek, "Unusually High Thermal Conductivity of Carbon Nanotubes", *Phys. Rev. Lett.*, vol. 84, no. 20, pp. 4613-4616, May 2000. doi: 10.1103/PhysRevLett.84.4613

[25] A. A. Balandin, S. Ghosh, W. Bao, I. Calizo, D. Teweldebrhan, F. Miao, and C. N. Lau, "Superior Thermal Conductivity of Single-Layer Graphene", *Nano Lett.*, vol. 8, no. 3, pp. 902-907, Feb. 2008. doi: 10.1021/nl0731872

[26] L. Li, Z. Zhu, T. Wang, J. A. Currivan-Incorvia, A. Yoon, and H.-S. P. Wong, "BEOL Compatible Graphene/Cu with Improved Electromigration Lifetime for Future Interconnects", *in IEDM Tech. Dig.*, 2016, pp. 240-243. doi: 10.1109/IEDM.2016.7838383

[27] J. R. Balck, "Electromigration-A Brief Survey and Some Recent Results", *IEEE Trans. Electron Devices*, vol. 16, no. 4, pp. 338-347, Apr. 1969. doi: 10.1109/T-ED.1969.16754

[28] E. Pop, D. Mann, J. Reifenberg, K. Goodson, and Hongjie Dai, "Electro-thermal transport in metallic single-wall carbon nanotubes for interconnect applications", *in IEDM Tech. Dig.*, 2005. doi: 10.1109/IEDM.2005.1609321

[29] M. Brandbyge, J.-L. Mozos, P. Ordejn, J. Taylor, and K. Stokbro, "Density-functional method for noneqilibrium electron transport", *Phys. Rev. B*, vol. 65, pp. 165401, Mar. 2002. doi: 10.1103/PhysRevB.65.165401

[30] J. M. Soler, E. Artacho, J. D. Gale, A. Garca, J. Junquera, P. Ordejn, and D. Snchez-Portal," The SIESTA method for ab initio order-N materials simulation", *J. Phys. Condens. Matter*, vol. 14, no. 11, pp. 2745, Mar. 2002. doi: 10.1088/0953-8984/14/11/302

[31] M. Griebel, S. Knapek, and G. Zumbusch, *Numerical Simulation in Molecular Dynamics*, Springer, 2007.

[32] M. Griebel and J. Hamaekers, Molecular dynamics simulations of the elastic moduli of polymercarbon nanotube composites, *Comput.Methods*

in Appl.Mech.Eng., vol. 193, no. 17-20, pp. 1773-1788, May 2004. doi: 10.1016/j.cma.2003.12.025

[33] K. D. Nielson, A. C. T. van Duin, J. Oxgaard, W. Deng, and W. A. Goddard, "Development of the ReaxFF reactive force field for describing transition metal catalyzed reactions, with application to the initial stages of the catalytic formation of carbon nanotubes", *J. Phys. Chem. A.*, vol. 109, pp. 493-499, Dec. 2005. doi: 10.1021/jp046244d

[34] Atomistix ToolKit version 2016.4, QuantumWise A/S. Available: http://www.quantumwise.com [Accessed Dec. 04, 2017].

[35] J. P. Perdew, K. Burke, and M. Ernzerhof, "Generalized Gradient Approximation Made Simple", *Phys. Rev. Lett.*, vol. 77, pp. 3865, Oct. 1996. doi: 10.1103/PhysRevLett.77.3865

[36] S. Grimme, J. Antony, S. Ehrlich, and H. Krieg, "A consistent and accurate ab initio parametrization of density functional dispersion correction (DFT-D) for the 94 elements H-Pu", *J. Chem. Phys.*, vol. 132, pp. 154104, Apr. 2010. doi:10.1063/1.3382344.

[37] P. Avouris, Z. Chen, and V. Perebeinos, "Carbon-based electronics", *Nat. Nanotech.*, vol. 2, pp. 605615, Sep. 2007. doi: 10.1038/nnano.2007.300

[38] A. D. Franklin and Z. Chen, "Length scaling of carbon nanotube transistors", *Nat. Nanotech.*, vol. 5, pp. 858-862, Dec. 2010. doi: 10.1038/NNANO.2010.220

[39] Jianshi Tang, Qing Cao, Damon B. Farmer, George Tulevski, and Shu-Jen Han, "Carbon nanotube complementary logic with low-temperature processed end-bonded metal contacts", *in IEDM Tech. Dig.*, 2016. doi: 10.1109/IEDM.2016.7838350

[40] Qing Cao, Shu-Jen Han, Jerry Tersoff, Aaron D. Franklin, Yu Zhu, Zhen Zhang, George S. Tulevski, Jianshi Tang, and Wilfried Haensch, "End-bonded contacts for carbon nanotube transistors with low, size-independent resistance", *Science*, vol. 350, no. 6256, pp. 68-72, Oct. 2015. doi: 10.1126/science.aac8006

[41] Juekuan Yang, Yang Yang, Scott W. Waltermire, Timothy Gutu, Alfred A. Zinn, Terry T. Xu, Yunfei Chen, and Deyu Li, "Measurement of the Intrinsic Thermal Conductivity of a Multiwalled Carbon Nanotube and Its Contact Thermal Resistance with the Substrate", *Small*, vol. 7, no. 16, pp. 2334-2340, Jun. 2011. doi: 10.1002/smll.201100429

[42] Baratunde A. Cola, Xianfan Xu, and Timothy S. Fisher, "Increased real contact in thermal interfaces: A carbon nanotube/foil material", *Appl. Phys. Lett.*, vol. 90, pp. 093513, Mar. 2007. doi: 10.1063/1.2644018

[43] K. M. Mohsin, A. Srivastava, A. K. Sharma, and C. Mayberry, "Characterization of MWCNT VLSI Interconnect with Self-heating Induced Scatterings", *in Proc. IEEE Comput. Soc. Annu. Symp. VLSI*, 2014, pp. 368373. doi: 10.1109/ISVLSI.2014.31

[44] E. Pop, D. A. Mann, K. E. Goodson, and H. Dai, "Electrical and thermal transport in metallic single-wall carbon nanotubes on insulating substrates", *J. Appl. Phys.*, vol. 101, no. 9, pp. 093710, May 2007. doi: 10.1063/1.2717855

[45] M. Jonson, and G. D. Mahan, "Mott's formula for the thermopower and the Wiedemann-Franz law", *Phys. Rev. B.*, vol. 21, no. 10, pp. 4223-4229, May 1980. doi: 10.1103/PhysRevB.21.4223

[46] Kittel, C., *Introduction to Solid State Physics.*, John Wiley and Sons, 2005.